Geochemical Perspectives Letters

Diffusional fractionation of helium isotopes in silicate melts

H. Luo, B.B. Karki, D.B. Ghosh, H. Bao

Supplementary Information

The Supplementary Information includes:

- Deep Potential Training
- Numerical Modelling of Diffusion
- Table S-1
- Figures S-1 to S-4
- Supplementary Information References

Deep Potential Training

We constructed the deep-learning potential (DP) models for helium-bearing albite and model basalt melt using the DP-GEN (Zhang *et al.*, 2020) scheme for the configurational space covering a temperature range 1400-4000 K and a volume range 1.0–1.1 V_a (V_a = 1435 Å^3) for helium-bearing albite melt and 0.89–1.09 V_b (V_b = 1389 Å^3) for helium-bearing model basalt melt. The DP-GEN scheme works iteratively, and each iteration includes three stages, exploration, labeling, and training. To begin with, rough DP models are first trained by a simple data set. The following are the details of our training setups.

Initial data set. We randomly picked 10 configurations (1 He + 8 $NaAlSi_3O_8$, 105 atoms for helium-bearing albite melt and 1 He + $Ca_9Mg_6Al_6Si_{18}O_{60}$, 100 atoms for helium-bearing model basalt melt) at each volume (1.0 V_a, 1.02 V_a, 1.05 V_a, and 1.1 V_a, where V_a = 1435 Å^3 for helium-bearing albite melt and 0.89 V_b, 0.94 V_b, 1.0 V_b, and 1.09 V_b, where V_b = 1389 Å^3 for helium-bearing model basalt melt) from first-principles molecular dynamics (FPMD) simulations as the initial configurations. Then short-time (40 femtoseconds) and high-precision (see the labeling step) FPMD simulations starting from each of the initial configurations were performed to generate the initial data set, which were labeled with energy and force.

Exploration. DP-based molecular dynamics (DPMD) simulations using the LAMMPS package (Plimpton, 1995) interfaced with the DeepMD-kit (Wang *et al.*, 2018) were performed to explore the configurational space. In each

iteration, canonical (*NVT*) simulations of 4 volumes as used in creating the initial data set and 6 temperatures (1400, 1700, 2200, 3000, 3500, 4000 K) were conducted. The time duration of these simulations increased from 1 to 10 picosecond (ps) with increasing iterations (*i.e.*, 1 ps in the first iteration, 3 ps in the second iteration, 6 ps in the third iteration, 10 ps in the fourth and remaining iterations until convergence). The explored configurations are categorized as failed, candidate, and accurate, according to the maximum deviation of forces (δ_f^{max}), defined as $\delta_f^{max} = \max_i \sqrt{\langle \|f_i - \langle f_i \rangle\|^2 \rangle}$, where f_i is the force acting on atom *i*, and $\langle \dots \rangle$ represents the average of the DP model ensemble. The failed and accurate sets include configurations with large force deviations ($\delta_f^{max} > \delta_{high}$) and small force deviations ($\delta_f^{max} < \delta_{low}$), respectively, where δ_{high} and δ_{low} are user-provided. The configurations with maximum force deviations between δ_{low} and δ_{high} are classified as candidates. A good convergence of the DP-GEN iterations is achieved when almost all the explored configurations are categorized as accurate. The lower and higher force deviations (δ_{low} and δ_{high}) were set to be 0.15 and 0.40 eV/Å for the first 8 iterations, 0.25 and 0.50 eV/Å for the second 6 iterations. In each iteration, 300 configurations in the candidate set were randomly picked and sent to the labelling stage.

Labelling. DFT calculations were conducted within local density approximation (Ceperley and Alder, 1980) and projector augmented wave method (Blochl, 1994; Kresse and Joubert, 1999) using Vienna Ab-initio Simulation package (Kresse and Furthmuller, 1996). We used a plane-wave cutoff energy of 700 eV and Gamma-point Brillouin-zone sampling. The convergence criterion of the self-consistent field (SCF) was set to be 10^{-6} eV.

Training. The smoothed version of DP (Zhang *et al.*, 2018) implemented in DeepMD-kit (1.2.0) (Wang *et al.*, 2018) was applied to train the potential energy surface. The sizes of the embedding and fitting networks were set to be (25, 50, 100) and (240, 240, 240). The radial cutoff was chosen to be 6.0 Å in the DP-GEN iterations. The start learning rate, decay rate, and decay steps were 0.001, 0.95, and 2000, respectively. In each iteration, four DP models were trained for 400, 000 steps with the same architecture and data set but different initial model parameters. After the DP-GEN iterations were converged, we generated the final DP model with a radial cutoff set to 7.0 Å and training steps set to 1,000,000 with the decay step set to 5000. A new exploration stage begins by using the newly trained DP models based on the updated data set.

In total, we performed 14 DP-GEN iterations and about 2.88 million helium-bearing albite melt configurations were explored, so as for helium-bearing model basalt melt. A small portion (~0.15 %) of them was selected for labeling. The percentage of configurations categorized as accurate in the exploration stage of the last iteration was around 99 %. With two well-trained DP models for the two melts, respectively, we first equilibrated the systems in the NPT ensemble at different temperatures (3000, 2200, 1700 K) and zero pressure to extract the corresponding cell volumes. Then we performed canonical (*NVT*) simulations for each He isotope. The volumes we obtained are V_a = 1570, 1535, and 1505 Å^3 at 3000, 2200, and 1700 K, respectively; V_b = 1390, 1338, and 1300 Å^3 at 3000, 2200, and 1700 K, respectively.

Numerical Modelling of Diffusion

The evolution of He concentration profile in melts during diffusive gas loss can be described by:

$$\frac{\partial C}{\partial t} = D\frac{\partial^2 C}{\partial^2 x},$$

where the initial concentration distribution is $C = C_0$ for all values of x and one boundary concentration distribution is $\partial C(x = 0,\ t > 0)/\partial x = 0$. Diffusivities of He in rhyolite and basalt melt at 1100 and 1400 K, respectively, are estimated by using our fitted Arrhenius relationship. Experimental and thermodynamic constraints on He elemental/isotopic systematics during magma degassing is largely absent. Here we assume that the He concentration in the vapour at the melt-vapour interface, $C(x = L,\ t > 0)$, is zero. This simplification may make sense as He is highly volatile and in the vapour He diffuses several orders of magnitude faster than that in the melt. A non-zero He concentration in the vapour at the melt-vapour interface affects the absolute values of model predictions but not the overall conclusions as shown in Figure 4. The evolution of $(^3He/^4He)/(^3He/^4He)_0$ and He loss ratio are calculated by adding up all the corresponding values in the melt. Our results for β equal to 0.5 are close to the one calculated for spherical geometry (Trull and Kurz, 1999), suggesting that the geometry does not affect the overall conclusions either.

Supplementary Tables

Table S-1 Diffusion coefficients of He isotopes in albite and model basalt melts at different temperatures around zero pressure. Estimated diffusivities of ^{4}He in albite and model basalt melts at 3000 K from 100 ps FPMD simulations are (69.8 ± 12.3) × 10^{-9} and (41.6 ± 5.6) × 10^{-9} m^2/s, respectively.

	T (K)	M_{He} (g/mol)	D_{He} (10^{-9} m^2/s)
albite	3000	1	124 ± 8
	3000	2	97.5 ± 3.2
	3000	3	84.6 ± 5.5
	3000	4	74.7 ± 7.2
	2200	1	64.9 ± 9.9
	2200	2	52.8 ± 1.9
	2200	3	46.4 ± 2.5
	2200	4	40.5 ± 2.6
	1700	1	49.9 ± 9.3
	1700	2	39.2 ± 6.3
	1700	3	35.5 ± 5.7
	1700	4	31.5 ± 5.9
model basalt	3000	1	67.5 ± 3.2
	3000	2	56.0 ± 1.6
	3000	3	47.6 ± 1.5
	3000	4	44.1 ± 1.7
	2200	1	27.6 ± 1.0
	2200	2	22.1 ± 1.7
	2200	3	20.2 ± 1.3
	2200	4	18.0 ± 0.6
	1700	1	8.72 ± 1.32
	1700	2	7.16 ± 0.69
	1700	3	6.65 ± 0.76
	1700	4	5.88 ± 0.63

Supplementary Figures

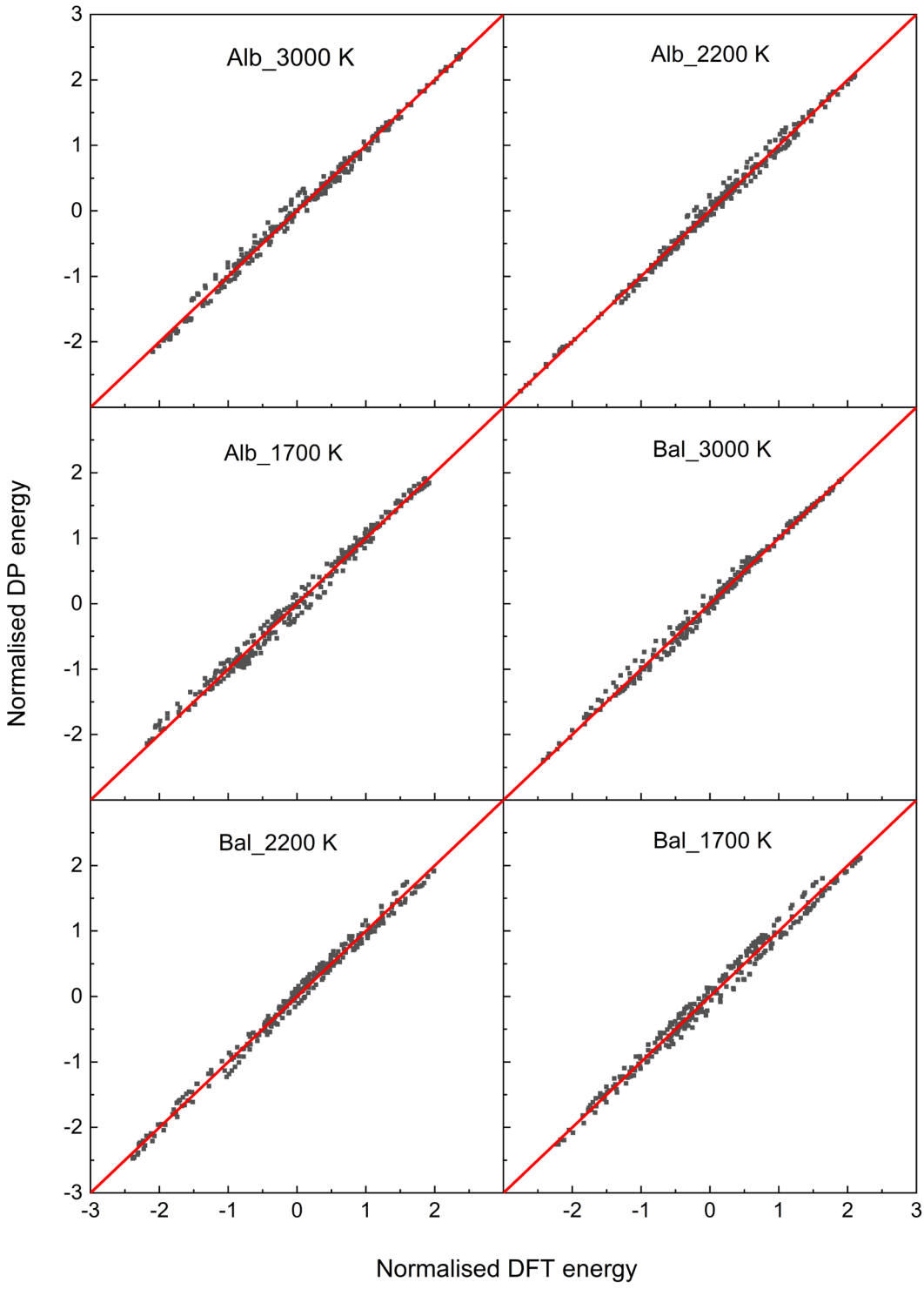

Figure S-1 Comparison of normalised energies calculated by deep potential (dp) and density functional theory (DFT) using a test data set.

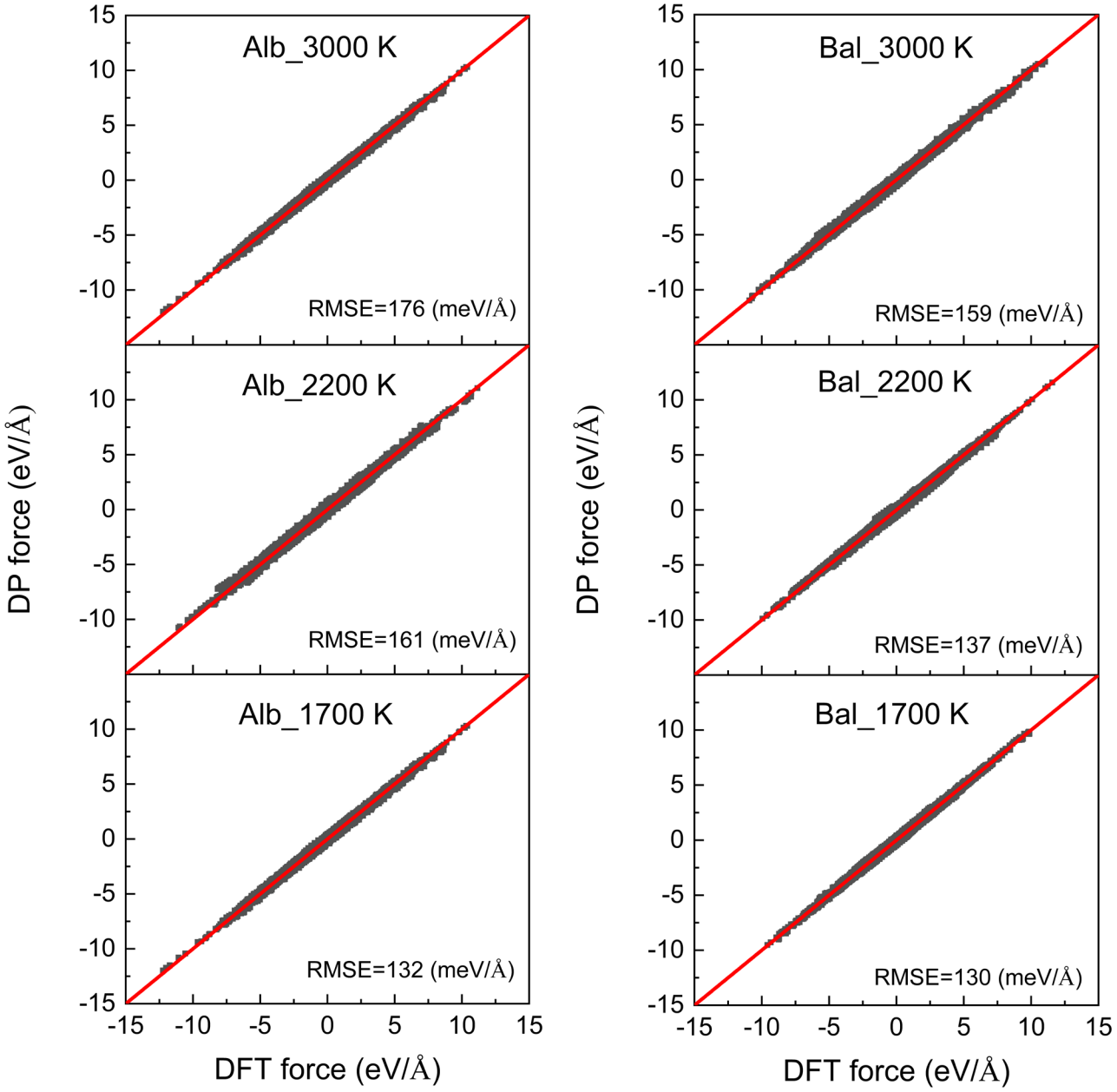

Figure S-2 Comparison of forces calculated by deep potential (dp) and density functional theory (DFT) using a test data set.

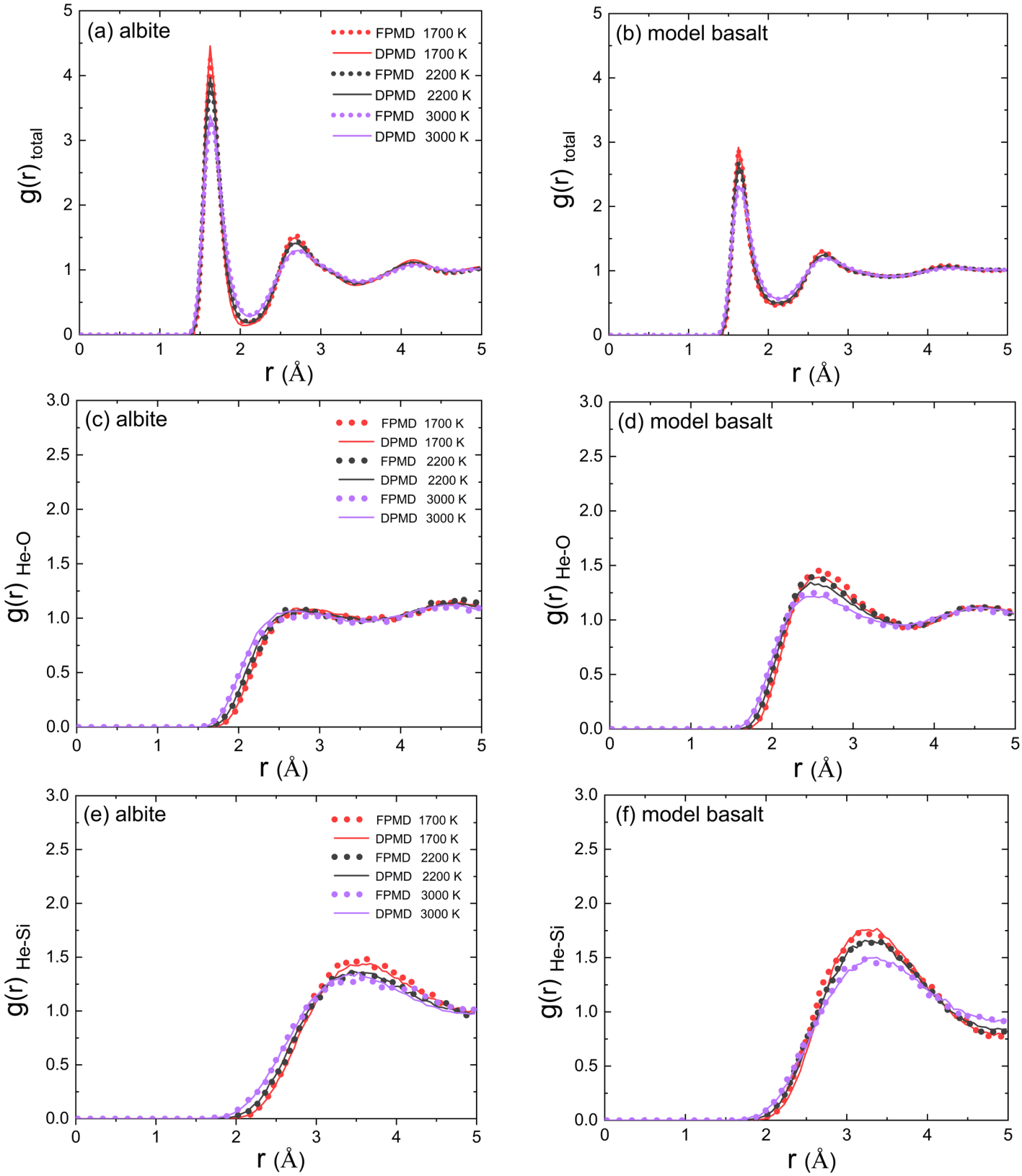

Figure S-3 Comparison of total **(a** and **b)** and partial **(c-f)** radial distribution functions calculated from DPMD and FPMD simulations. The FPMD data is more scattered due to limited sampling (50–150 ps).

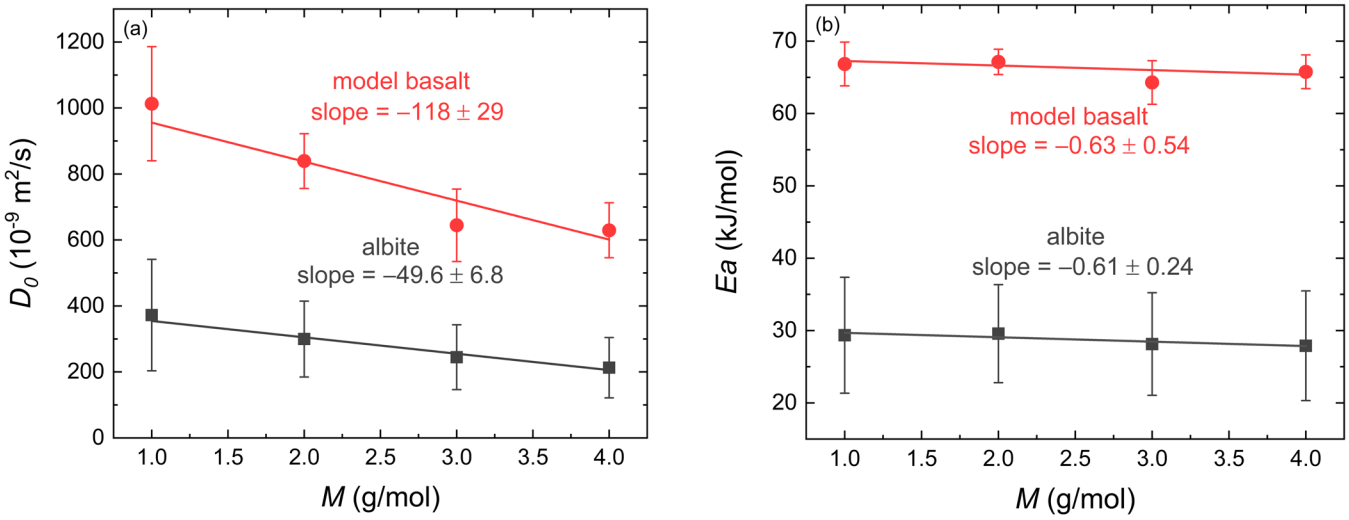

Figure S-4 The predicted pre-exponential factor ($D_{0\alpha}$) and activation energy (E_α) of He isotopes as a function of isotopic mass in albite and model basalt melts.

Supplementary Information References

Blochl, P.E. (1994) Projector Augmented-Wave Method. *Physical Review B* 50, 17953-17979.

Ceperley, D.M., Alder, B.J. (1980) Ground-State of the Electron-Gas by a Stochastic Method. *Physical Review Letters* 45, 566-569.

Kresse, G., Furthmuller, J. (1996) Efficiency of ab-initio total energy calculations for metals and semiconductors using a plane-wave basis set. *Computational Materials Science* 6, 15-50.

Kresse, G., Joubert, D. (1999) From ultrasoft pseudopotentials to the projector augmented-wave method. *Physical Review B* 59, 1758-1775.

Plimpton, S. (1995) Fast Parallel Algorithms for Short-Range Molecular Dynamics. *Journal of Computational Physics* 117, 1-19.

Trull, T.W., Kurz, M.D. (1999) Isotopic fractionation accompanying helium diffusion in basaltic glass. *Journal of Molecular Structure* 485, 555-567.

Wang, H., Zhang, L.F., Han, J.Q., E, W.N. (2018) DeePMD-kit: A deep learning package for many-body potential energy representation and molecular dynamics. *Computer Physics Communications* 228, 178-184.

Zhang, L.F., Han, J.Q., Wang, H., Saidi, W., Car, R., E, W. (2018) End-to-end symmetry preserving inter-atomic potential energy model for finite and extended systems. *Advances of the Neural Information Processing Systems*, 4441-4451.

Zhang, Y.Z., Wang, H.D., Chen, W.J., Zeng, J.Z., Zhang, L.F., Wang, H., E, W. (2020) DP-GEN: A concurrent learning platform for the generation of reliable deep learning based potential energy models. *Computer Physics Communications* 253.